Polymer(Korea) Vol. 20, No. 5, pp 753-768(1996)

Fragmentation 시험법과 비파괴 Acoustic Emission을 이용한 내열성이 있는 SiC 섬유강화 열가소성 복합재료의 계면물성 및 미세 파괴구조에 관한 연구

박 종 만† · 정 의 민 · 신 외 경 · 이 상 일 · 윤 동 진* 이 준 현**

경상대학교 고분자공학과, *한국표준연구소 재료물성평가센타, **부산대학교 기계설계공학과

(1996년 4월 26일 접수)

Interfacial Properties and Micro-Failure Mechanisms of SiC Fiber Reinforced High Temperature Thermoplastic Composites Using Fragmentation Technique and Acoustic Emission

Joung-Man Park†, Eui-Min Chong, Wae-Gyeong Shin, Sang-Il Lee, Dong-Jin Yoon*, and Joon-Hyun Lee**

Dept. of Polymer Science & Engineering and RIIT, Gyeongsang National University, Chinju 660-701, Korea

**Center for Materials Evaluation, Korea Research Institute of Standards and Science, Taedok Science Town, Taejon 305-306, Korea*

***Dept. of Mechanical Design Engineering, Pusan National University, Pusan 609-735, Korea*

(Received April 26, 1996)

요 약: Nicalon SiC fiber/polycarbonate (PC) composite에서의 amino-silane coupling agent (γ-(aminopropyl)trimethoxysilane)의 효과를 알기 위해 dual fibers composites (DFC) 시편을 이용하여 계면전단강도를 측정하였다. DFC 시편 제조와 silane coupling agent 처리의 최적조건을 구하였다. SiC 섬유의 인장강도에 대한 통계적 분포를 주로 Weibull분포의 방법을 이용하여 비교하였다. SiC 섬유의 표면에 불균일하게 존재하는 flaws로 인해, 인장강도와 연신율은 gauge 길이가 짧을수록 큰 값을 보였다. SiC 섬유와 PC 매트릭스간의 계면전단강도는 건조 상태에서 약 150%의 큰 증가를 보였으며, 환경에 대한 영향을 평가하기 위해 85 ℃의 물에 75분간 담근 후 건조 상태와 동일한 방법으로 실험한 경우 약 170% 정도의 증가치를 보였다. 그 이유는 SiC 섬유와 PC 매트릭스의 다른 두 계면간에서의 화학적 혹은 물리적 결합에 기인한 것으로 여겨진다. Acoustic emission (AE) 시험법을 통하여 SiC 섬유와 PC 매트릭스간의 잘 분리된 두 분포를 보여 주었으며, FFT (fast Fourier transform) 분석을 통하여 섬유와 매트릭스의 failures에 대한 특징적인 주파수를 확인하였다. AE events와 섬유파단 간의 일-대-일 대응 관계를 확인함으로써 DFC 시험법보다 계면전단강도를 보다 쉽게 구할 수 있는 또 다른 방법이 될 수 있으며, 불투명한 시편들에도 적용시킬 수 있을 것으로 생각된다.

ABSTRACT: Interfacial shear strengths (IFSS) between fiber and matrix in dual SiC fibers reinforced polycarbonate (PC) composites (DFC) were investigated by the fragmentation method and acoustic emission (AE) technique. Statistical analysis of SiC fiber tensile strength was performed mainly in terms of Weibull distribution. Tensile strength and elongation for SiC fiber decreased with increasing gauge lengths, due to heterogeneous distribution of flaws on the fiber surface. Using amino-silane coupling agent, the IFSS showed significant improvement in the range of 150% under dry conditions. On the other hand, investigating the environmental effects under wet condition (immersed in hot water at 85 ℃ for 75 min.), IFSS was improved about 170%. It is probably due to chemical and hydrogen bonds in two

different interphases in SiC fiber/silane coupling agent/PC matrix system. *In-situ* monitoring of AE during straining DFC specimens showed the sequential occurrence of two distinct groups of AE data. The first group might have come from SiC fiber breakages, and the second probably comes from mainly PC matrix cracking. Characteristic frequencies coming from the failures of fiber and PC matrix were shown via fast Fourier transform (FFT) analysis. By setting an appropriate threshold level, a one-to-one correspondence between the number of AE events and fiber breakages was established. This AE method could be correlated successfully to the IFSS via the fragmentation technique, which was also applied to the nontransparent specimens.

Keywords: *interfacial shear strength, amino-silane coupling agent, acoustic emission, fragmentation test, one-to-one correspondence.*

INTRODUCTION

Recently, advanced polymeric composites using thermoplastic resins such as polycarbonate, polyetheretherketone, polyimide are being developed rapidly due to the feasibility of recycling from the areas of the commercial industries to aerospace applications.[1-4] These efforts are being undertaken to replace thermoset resin such as epoxy with the advanced thermoplastics.

Interfacial shear strength (IFSS) between fiber and matrix is a very important factor to determine mechanical performance for composite materials. If the IFSS is too low, it is hard to expect the performance of the reinforced fibers in composites, whereas if the IFSS is too high, there may occur stress crack propagation. It is necessary that the IFSS should be determined via optimization in accordance with the final purpose.

IFSS in fiber reinforced composites can be improved by introduction of chemical functions after oxidation or plasma treatment of fiber surface and/or by use of commercial coupling agents for compatibility of fiber and matrix.[5-7] Measuring the IFSS between fiber and matrix requires special techniques. Several micromechanical techniques have been proposed for measuring the IFSS in fiber reinforced composites for both thermoplastic and thermosetting resins. Some of the most frequently used techniques include the single fiber pull-out test,[8] the single fiber composites (SFC) test,[5,9,10] and the microindentation method[11] etc.

SFC test method, originally proposed by Kelly and Tyson[12] for the fiber/metal composites, can provide abundant statistical informations, e.g., the interfacial failure mode and the IFSS value using only several specimens. Base on the force balance in a micromechanical model, Kelly and Tyson showed that the IFSS, τ is given by

$$\tau = \frac{\sigma_f \cdot d}{2 \cdot L_c} \quad (1)$$

, where d is the fiber diameter, σ_f is the fiber fracture stress, and L_c is the critical fragment length. Since the actual fragment lengths and the fiber strengths are not constant but are strongly dependent on the gauge length, Eq. (1) can be modified by

$$\tau = \frac{\sigma_f \cdot d}{2 \cdot L_c} \cdot K \quad (2)$$

, where σ_f is the fiber tensile strength at a gauge length equal to the mean fragment length, L_c and K is the coefficient which depends on the variation.[13] If the fragment lengths vary between $L_c/2$ and L_c, $K=0.75$ can be taken as a mean value. Since distribution of fragment lengths is observed experimentally, Drzal et al.[14] altered the equation to reflect Weibull statistics to the form,

$$\tau = \frac{\sigma_f}{2 \cdot \beta} \cdot K \qquad (3)$$

$$K = \Gamma\left[1 - \frac{1}{\alpha}\right]$$

where β is the shape parameter, α is the scale parameter and Γ is the Gamma function. In a more vigorous analysis using the Monte Carlo simulation Phoenix and Netravali[10] proposed that

$$K = \left[\frac{\Lambda}{2}\right]^{(1+m)/m} \qquad (4)$$

, where the nondimensional parameter, Λ represents the mean aspect ratio, $L/L_0 \cdot L_0$ is the characteristic length varying between 1.34 (for $m \rightarrow \infty$) and 1.96 (for $m=3$ which is typically the smallest value in the experiment). Therefore, K varies between 0.67 for very large m and 0.97 for $m=3$.

Silane coupling agents are usually known to improve interfacial performance in glass fiber reinforced composites under ambient and especially under highly humid conditions. It allows the retention of the adhesion between fiber-matrix in the event of any ingress of water to the interface due to enhanced physical, mechanical and/or chemical bonding between the glass fiber and polymer matrix.[5,6]

Acoustic emission (AE) is one of the very sensitive nondestructive testing (NDT) methods. The AE can monitor the fracture of composite structure, and the characteristics of AE parameters help understanding the types of deformation sources or process that are active. Fiber reinforced plastics (FRP) involve mainly three types of failure mechanisms: i.e., fiber fracture, matrix cracking and fiber-matrix interphase debonding. Material properties of fiber and matrix are obviously important factors governing failure process. According to Ma,[15] an analysis of envelope signals of the AE produced from carbon fiber/PC composites showed a one-to-one correspondence between AE signals and fiber fractures. AE technique can also be adopted to nontransparent polymer matrix including metal and ceramic matrix composites.[6] The matrix can be dissolved chemically or burned off to know the fragment lengths of fibers in matrix.

Most of SFC works[5,10] have been applied to the thermosetting composite so far except for a few thermoplastic SFC works[9,16] recently. In this work for the dual SiC fibers/thermoplastic PC composite, effects of surface treatments on the IFSS using amino-silane coupling agent and micro-failure mechanisms were evaluated with the aids of fragmentation method and AE technique. The effect of amino-silane on the durability in the IFSS was compared under wet and dry conditions. Chemical structures of the silane on the SiC fiber surfaces were characterized to understand interphases between SiC fiber and PC matrix. Using the DFC specimens, AE method was applied to characterize the failure mechanisms of SiC/PC specimens while being strained. Those results were correlated with each other.

EXPERIMENTAL

Materials.

SiC Fiber: The used SiC fiber was ceramic grade silicon carbide fiber manufactured by Nippon Carbon Co. Ltd. under the name of Nicalon. Fibers without sizing agent were obtained in the form of a tow containing 500 filaments. After cutting into about 350 mm long pieces from the fiber tow, single fibers were carefully extracted. A typical composition of a Nicalon fiber was Si 58.3%, free carbon 30.4% and oxygen 11.1% by weight etc.[17] Average SiC fiber diameter was 13.5 μm. The fiber tensile strength was about 3000 MPa and the elastic modulus was 170 GPa.

Amino-Silane Coupling Agent: Amino-silane coupling agent (γ-(aminopropyl)trimethoxysilane) was purchased from Aldrich Chemical Co. and was used without further purification. Amino-silane coupling agent was diluted to the required concentration in aqueous solution for the treatment of SiC fiber surfaces. The chemical structure of amino-silane coupling agent is $N_2HCH_2CH_2CH_2Si(OCH_3)_3$.

Polymer Matrix: The matrix was polycarbonate, which was granularly supplied from Sam Yang Hwasung Co. (grade No. 3025). Granule sizes were about 1-2 mm. Polycarbonate is mostly amorphous polymer and characterized by the -COO- unit and rings in its chain. The melting point (T_m) and the glass transition temperature (T_g) are around 245 ℃ and 145 ℃, respectively. Tensile modulus of bulk PC polymer was about 1.32 GPa. For a mold releasing film, a commercially available polyimide film (Air-tech. International Co., U. S. A.) was used.

Methods.

Measurements of Single Fiber Tensile Strength: The mean diameter of about 50 SiC fibers was determined using an optical microscope (Nixon model: HEX-DX) with a calibrated eye piece. Diameters of several fibers were measured at three different points to identify the diameter scattering. They were made by placing the single fiber onto straw-board frame. It was fixed by Scotch tape in the center line on both ends, and subjected to hardening by means of epoxy curing adhesives. The tensile strength measurement was carried out at cross-head speed of 0.5 mm/mn and small capacity 100 N load cell for the Universal Testing Machine (Lloyd instruments Ltd., LR 5K). Five different gauge lengths were chosen as 2, 5, 10, 20 and 100 mm for both the untreated and the silane-treated. About forty specimens were tested for each gauge length to calculate reliable statistical mean values using Weibull distribution.

Surface Treatment Using Amino-Silane Coupling Agent: Main experimental procedure was the dip-coating of the fiber surface in amino-silane coupling agent solution. Amino-silane coupling agent was diluted in the distilled water with pH 3.5 acidic condition. Silane solutions were prepared with various 0.5, 1, 2 and 5 wt% concentrations. SiC fibers were fixed individually in a steel frame and then were dipped into amino-silane solution for 1 min. to ensure uniform coating and to avoid the complication from the interaction of neighboring fibers in a frame. After fibers were coated, they were dried in the air for 3 hours at room temperature. The surfaces of treated SiC fiber were observed using scanning electron microscope (SEM, JEOL JSM6400). Fibers were sputter coated with gold for 100 seconds.

Dual Fibers Composite (DFC) Specimens Preparation: The dimension of specimen was 3 mm wide, 25 mm gauge long, and about 1 mm thick as shown in Fig. 1(a). DFC specimens were made by the untreated and the treated SiC

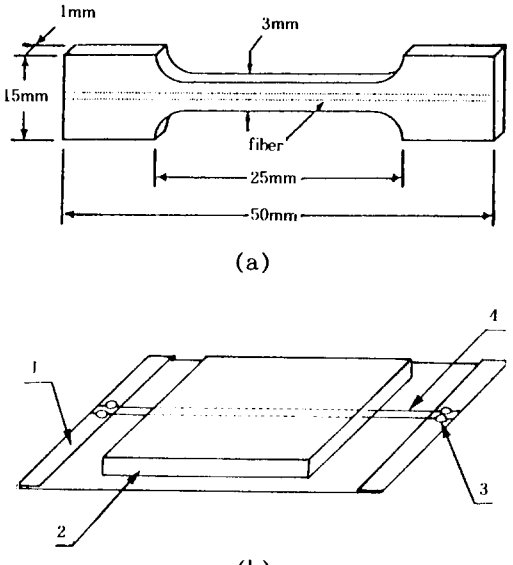

Figure 1. (a) Dimension of dog-bone shaped dual fibers composite (DFC) specimen and (b) Preparation of dual fibers composite (DFC) from polycarbonate.(1: aluminum foil, 2: granular layer, 3: kapton tape, 4: fiber).

fibers embedded with molten matrix polymer on the hot plate (Fig. 1(b)). First, dual SiC fibers were fixed using polyimide Kapton tapes on a sheet of aluminum plate of 1 mm thick. The granular typed-PC was melted on the frame for various melt temperatures and holding times. After melting, it was dipped into cold water quickly. Then, the specimen was cut using sharp knife, where dual fibers were run along the center axis, to produce a dogbone-shaped and correctly sized specimen. After fiber was positioned and straightness were checked with an optical microscope, misaligned specimens were discarded. Two fibers can act as reinforcing materials independently by separating with a certain distance apart in same matrix without interacting with each other. Mechanical properties on cooling procedures of the PC specimen without embedding fiber were obtained using universal testing machine (Lloyd instruments Ltd.: LR 5 K, 5 kN load cell) via the stress-strain curve.

Fourier Transform Infrared (FT-IR) Spectroscopy: Chemical analysis of silane treated-surfaces and PC matrix was performed by FT-IR spectroscopy (Bruker IFS66 FT-IR spectrometer). A thin coating of the condensed silanes was applied on KBr pellet using very pure KBr powder. A thin polymer film was made by melt casting between two KBr pellets under suitable pressure at the melting temperature. The number of scans was chosen to be 20 for both background and samples.

Interfacial Shear Strength (IFSS) Measurements: The DFC fragmentation test was carried out to obtain the IFSS value using a specially designed strain fixture mounted under the optical microscope. Fig. 2 illustrates the schematic representation of the fiber was fragmentation under progressively increasing load and the corresponding fiber axial stress profile.[10] During testing, the specimen was incrementally stressed and the fiber was fractured into small segments within the matrix. As higher tensile stress is applied, the fracture process continues until no longer fracture occurs in the fiber. At this strain an ultimate fragment length attains critical length, L_c. Ultimate fragment lengths within the matrix were measured and subsequent failure process was observed via a polarized-light microscopy. The locus of failure is identified and the process is replicated *in situ* events in the actual composite.

The classical relationship among fiber tensile strength σ_f, critical fragment length to diameter ratio (i. e., aspect ratio, L_c/d) and the IFSS, τ was given by Kelly-Tyson.[12] However, widely-distributed τ values are obtained as a result of random distribution and heterogeneities of flaws in the fibers. The data for both fragment length and fiber strength may be approximated by

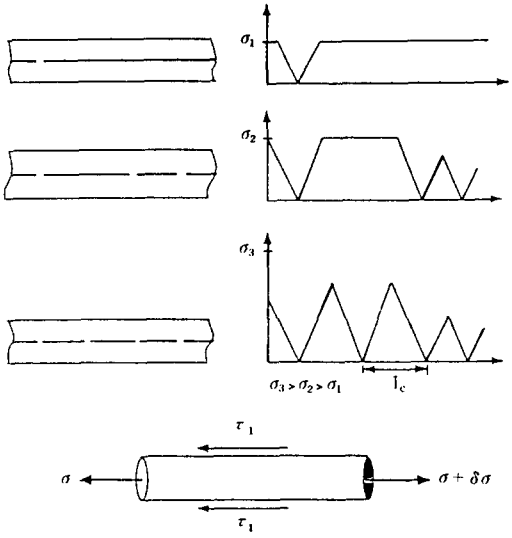

Figure 2. Graphic representation of the evolution of failures and the corresponding stress profiles in the embedded fiber during fragmentation test.

Weibull distribution and these distributions can be combined to calculate the IFSS. The cumulative probability of failure of a fiber length L loaded to stress level σ is given by[18]

$$F = 1 - \mathrm{Exp}\left[- L(\frac{\sigma}{\sigma_0})^m \right] \quad (5)$$

, where σ_0 is the scale parameter, m is the shape parameter (or Weibull modulus), the mean value of estimated probability, and F is assigned as

$$F = \frac{i}{N+1} \quad (6)$$

, where N is the total number of fiber fragments, and i is the recording number. In order to evaluate the parameters m and σ_0, eq. (6) can be rearranged into a linearized form as

$$L_n [-L_n(1-F)] = \beta L_n (t) - \beta L_n \alpha \quad (7)$$

Thus, a plot of $L_n [L_n (1-F)]$ versus $-L_n$ (aspect ratio) yields a straight line whose slope and intercept yields β and α, respectively. From eq. (7), the IFSS can be calculated as

$$\tau = \frac{\sigma_f}{2 \cdot \beta} \cdot \Gamma\left[1 - \frac{1}{\alpha}\right] \quad (8)$$

, where Γ represents the Gamma function, β and α are shape and scale parameter, and σ_f is single fiber strength at the critical length, L_c. To know values at the critical length, a direct fiber tensile test at such short lengths can result in experimental difficulties.[19] Fiber strengths are usually determined by macroscopic gauge lengths, and then with subsequent extrapolation to smaller gauge lengths using the Weibull weakest link rule. The tensile strength at a critical length is

$$\frac{\sigma_f}{\sigma_0} = \left(\frac{L_c}{L_0}\right)^{-\frac{1}{\rho}} \quad (9)$$

, where σ_0 is the fiber strength at gauge length L_c, and ρ is the shape parameter of the Weibull distribution for fiber strength.[20] In order to evaluate the effect of moisture exposure on IFSS, the DFC specimens were immersed in distilled water at 85 ℃ for 75 min. The IFSS of the specimen was then measured after equilibration for one hour at room temperature.

Acoustic Emission Measurements:. By using an AE analyzer (model AET5500 by HSBIT), AE tests were conducted during tensile test using a specially designed tensile device. Fig. 3 shows a schematic illustration of AE generation, detection and analytic system. A piezoelectric transducer was attached to the middle of the specimen. AE signals were detected by a wideband typed-piezoelectric transducer (model WD by PAC) with maximum sensi-

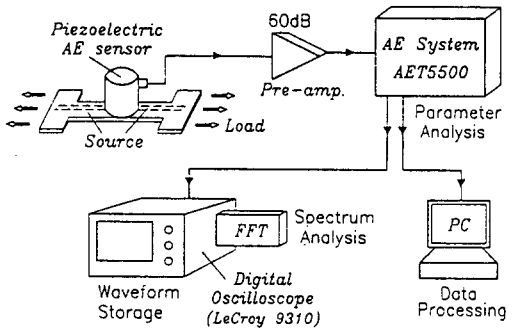

Figure 3. Schematic illustration of acoustic emission generation, detection and analytic system.

tivity of -60 dB (ref. 1 V/μ bar) at 550 KHz. The transducer was attached to the middle of the specimen using a couplant properly. The output signal from the AE sensor was amplified by 60 dB at preamplifier. Then it was fed into an AE signal processing unit, AET5500 system. The preamplifier output was also fed into a digital storage oscilloscope for the waveform analysis. The threshold level was set to 100 μV at the sensor. AE parameters such as event, peak amplitude, and energy were investigated for the time and distribution analysis. In addition, frequency analysis was performed by using the fast Fourier transform (FFT) to identify the characteristic peaks of frequency components for the failure sources.

RESULTS AND DISCUSSION

Statistical Analysis of SiC Fiber Tensile Strength, and Effects on Preparation Conditions of the DFC Specimen. Tensile strengths of most fibers are known to be dependant on the gauge length due to the probability of flaws along the fiber surfaces. Most ceramic fibers, for example SiC fiber is brittle and is susceptible to deteriorate the tensile strength due to surface flaws. The distribution of SiC fiber tensile strength exhibits relatively broad. In addition, uncareful handling can make the fibers to be intimately contacted, thus introducing new surface flaws. It also can reduce the fiber strength significantly.

Table 1. Tensile Strength and Elongation of Untreated SiC Fiber with (a) Various Gauge Lengths and (b) Concentration of Amino-silane

gauge length (mm)/ conc.(wt%)	number of specimens (EA)	diameter (μm)	tensile strength (MPa)	elongation (%)
2	35	13.3	3498(1212)*	4.51(1.91)
5	43	13.6	3299(847)	2.54(0.86)
10	34	14.0	3175(1052)	2.27(0.89)
20	39	13.5	2666(707)	1.39(0.30)
100	40	13.6	2108(617)	0.92(0.18)
untreated	35	13.3	3498(1212)	4.51(1.91)
0.5	33	13.9	5187(1238)	7.49(1.64)
1	39	13.4	5202(1473)	7.49(2.43)
2	34	13.9	4758(1189)	7.48(2.20)
5	35	13.8	4594(1395)	6.39(1.55)

* Parenthesis is standard deviation.

Table 1 showed the tensile strength and the elongation of untreated SiC fiber with (a) various gauge lengths and (b) silane concentrations. Both the tensile strength and the elongation decrease with an increasing gauge length. Due to randomly distributed flaws on the fiber surface, a size effect appeared. In Table 1(b), SiC fiber coated with amino-silane showed higher tensile strength and elongation values than the uncoated SiC fiber. It may be due to flaw healing effect on the defected fiber surfaces. At higher conc. more than 2 wt%, tensile strength decreased again due to stress concentration at lump-shaped coating portion.

Table 2 showed the fiber strengths for the untreated and the 1 wt% amino-silane treated with various gauge lengths. As the gauge length became smaller, the improvement in the fiber strength became larger. The healing effect on the defect sites due to silane coating may be more uniform in the range of short gauge

Table 2. Improvement in Single Fiber Strength under Various Gauge Length for the 1 wt% Amino-silane Coupling Agent Treated Fibers Compared with the Untreated Fibers

gauge length (mm)	untreated (MPa)	treated (MPa)	improvement (%)
2	3498	5202	49
5	3299	4420	34
10	3175	3860	22
20	2666	3171	19
75	–	2585	–
100	2108	–	–

* Improvement % = (treated − untreated)/(untreated) × 100.

length, whereas in long gauge length the uniformity of coating is reduced comparatively.

The unimodal distribution based on the single type of defects does not sometimes fit well with the experimental data. A multimodal distribution is required if there are more than one defect types. SiC fiber is known to have a multimodal strength distribution due to the different types of flaws.[21] One of them is a surface flaw such as a pit, and the other is an internal flaw such as a void. The internal defects were considered to be related to the tensile strength at short gauge lengths.

Fig. 4 showed statistical distributions (a) with four different gauge lengths and (b) with five different silane concentrations. As gauge length increases, tensile strength shifted toward lower and exhibited narrower distributions. Amino-silane treated SiC fiber exhibited higher strength distribution than the untreated SiC fiber probably due to the flaw healing effect on defected fiber surfaces.

Table 3 showed the fiber shape and the matrix condition for DFC specimens as functions of melting temperature and time. An optimum melting temperature was in the range of 250 to 270 ℃. Since PC matrix was too melted on 270 ℃, SiC fiber shape to be curvedly. Fig. 5 showed the stress-strain curves of dogbone

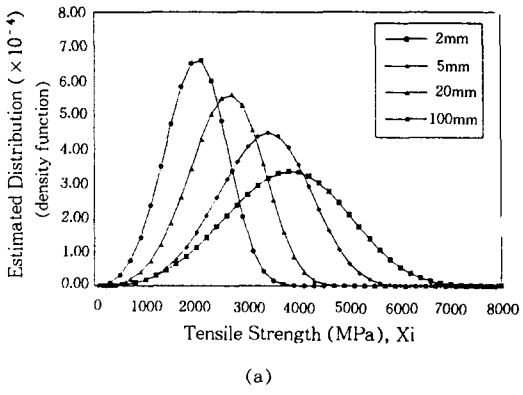

Figure 4. Comparison of the single fiber strength from the untreated fibers (a) with various gauge lengths and (b) with various concentrations.

Table 3. Effect on Preparation Conditions of DFC Specimens for Various Heating Time on the Hot Plate

heating temp. (℃)	heating time (min)	fiber shape in DFC	PC matrix condition
240	40	–	not melted
250	60	straight	melted
270	40	straight	melted
270	100	curve	too melted
300	40	curve	degradation

shaped PC specimens using two different cooling methods. In slow cooling, elongation was relatively small, because less ductile specimen was broken before necking to start. On the other hand, quick cooling showed much larger elonga-

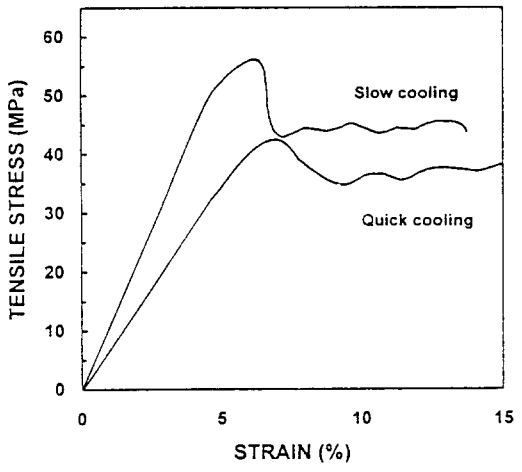

Figure 5. Stress-strain curve of dog-bone shaped polycarbonate specimens using two different cooling methods.

tion value. This is due to the occurring necking based on the minimized deterioration of plastic properties by the suitably-short melting time. Tensile moduli from two initial slopes in the curves were 1.32 GPa and 1.45 GPa for quick and slow cooling procedures, respectively.

Amino-Silane Interlayer. One of the principal experimental parameters for the optimized silane treatment on the fiber surface is concentration, although there are other parameters such as treating time, temperature, solvent. Uniformity of amino-silane coating was observed via SEM in Fig. 6. SEM photograph of the coated amino-silane showed relatively uniform when suitable 1 wt% amino-silane aqueous solution was used. At 5 wt% silane concentration, however, the formed coating was in lump shape. It can cause a weak boundary layer when fibers are embedded in the PC matrix. Amino-silane coupling agent can provide a molecular bridge between the SiC fiber and matrix. It was studied previously[7] that the thickness of coated silane on the treated fiber is significantly dependent on the silane concentration than on the dipping time in the treating solution.

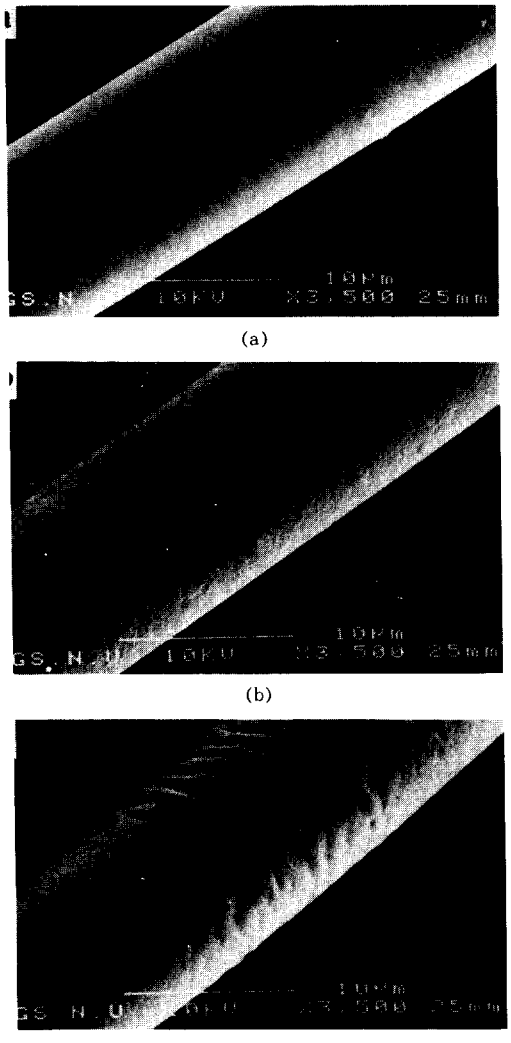

Figure 6. SEM photographs of SiC fibers: (a) untreated, (b) amino-silane treated (1 wt%, 1 min), and (c) amino-silane treated (5 wt%, 1 min).

In Fig. 7, FT-IR spectrum of (a) neat amino-silane is compared with (b) the spectrum obtained after drying at 25 ℃. The band due to Si-O-C appears at 817 cm^{-1}. The symmetric C-H stretching band at 2936 cm^{-1} is shown in Fig. 7(a), and the peak at 976 cm^{-1} appears due to the SiOH group. The band at 1084 cm^{-1} due to

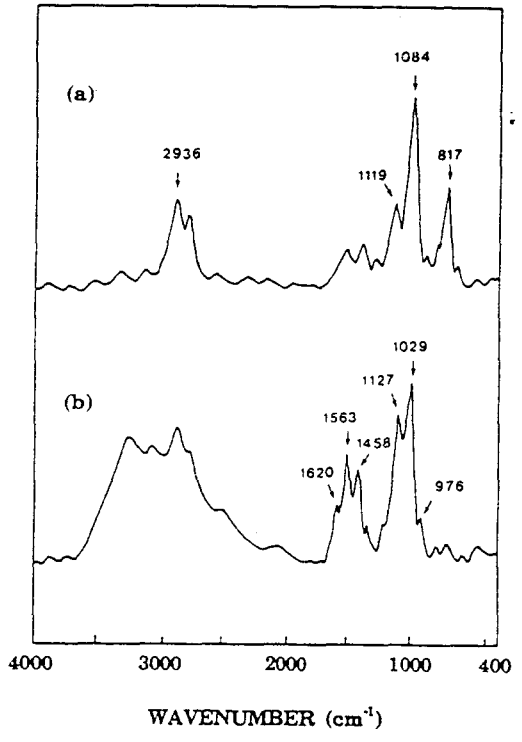

Figure 7. FT-IR spectra of (a) neat amino-silane and (b) amino-silane film after drying at 25 ℃ for 3 hours.

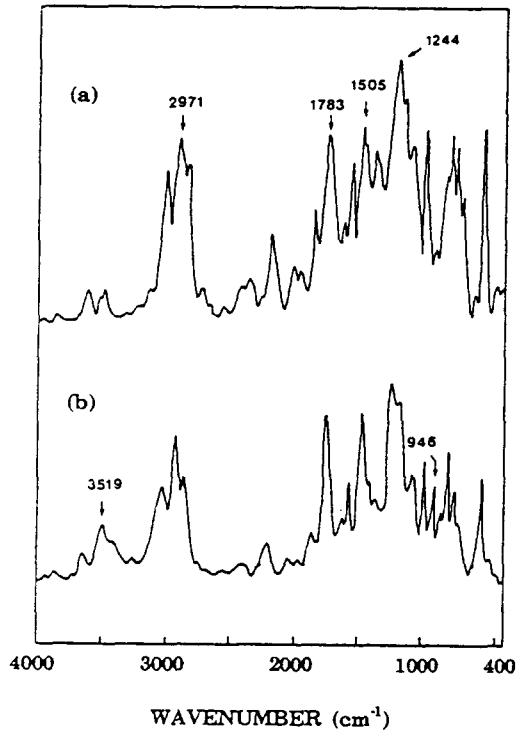

Figure 8. FT-IR spectra of (a) polycarbonate and (b) amino-silane/polycarbonate.

methoxy group ($-OCH_3$) disappeared after drying at room temperature. The condensation of silane is seen in the appearance of two very strong bands at 1029 and 1127 cm^{-1} due to the asymmetric Si-O-Si stretching vibrations. In addition, bicarbonate peaks appear at 1458, 1563 and 1620 cm^{-1} after drying in air.

In Fig. 8, spectrum (a) of the PC was compared with spectrum (b) obtained after reacting with amino-silane. The peak at 1244 cm^{-1} is due to ester group vibration. The appearance of a band at 3519 cm^{-1} is due to -OH and -NH- groups, as expected from the chemical reaction between PC and amino-silane.

Interfacial Shear Strength (IFSS) in DFC Specimens. Fragment lengths embedded in DFC specimen became smaller with increasing strain, because matrix around long-broken fiber still transfer stress to the SiC fiber. The first SiC fiber breakage usually occurred at a relatively low strain, around 1 %. In Fig. 9,

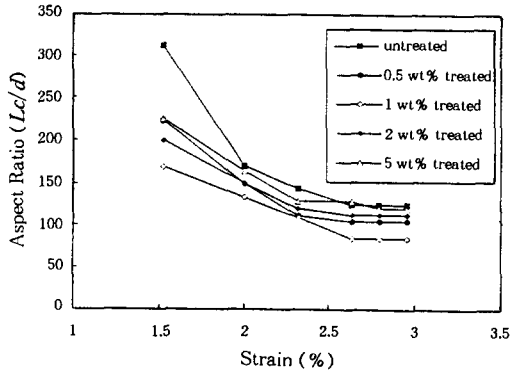

Figure 9. The relationship between aspect ratio and applied tensile strain with various concentration treated SiC fibers.

there is a plot for aspect ratio versus applied tensile strain with various silane concentrations. As strain increases, the aspect ratio generally decreases for the all cases. Initial drop in aspect ratio was steep, then was almost flat. This means that the critical average fragment length become reached. The 1 wt% treated SiC fiber showed the smallest aspect ratio among the other concentrations, which means the highest IFSS.

In Fig. 10, Weibull distributions of aspect ratio were plotted for the untreated and 1 wt% treated specimens under dry and wet conditions, respectively. In the treated cases distribution curves of aspect ratio were shifted to downward under dry and wet conditions. Effectiveness of amino-silane treatment also appeared in retaining adhesion between SiC fiber and PC matrix under wet condition after exposure to hot water. Table 4 listed Weibull distribution parameters for the aspect ratio, L_c/d and their IFSS for the untreated and the silane-treated SiC fibers under dry and wet conditions. Since aspect ratio value is directly related to the IFSS, it is easily shown that the smaller aspect ratio is, the higher the IFSS is. Shape parameter, β decreased up to 1 wt% silane concentration, then increased again to 5 wt% under dry and wet conditions.

Fig. 11 showed the improvement in the IFSS of SiC fibers under dry and wet conditions with various amino-silane concentrations. IFSS improvements were such high in the range of about 150 to 170% at 1 wt% concentration under both dry and wet conditions. Optimized treating concentration could be obtained as explained previously. Beyond this concentration, the IFSS decreased again due to lump-shaped thick coating. Although the same coupling agent is used, there are significant differences in the improvement effect on the IFSS as a function of adsorption amount. Properly chosen coupling agent based on the chemical functional groups between fiber and matrix can be said not to be the unique parameters to determine the IFSS.

Such high improvements can be due to chemical and/or physical bonding in two interphases in composites. Two interphases can be consid-

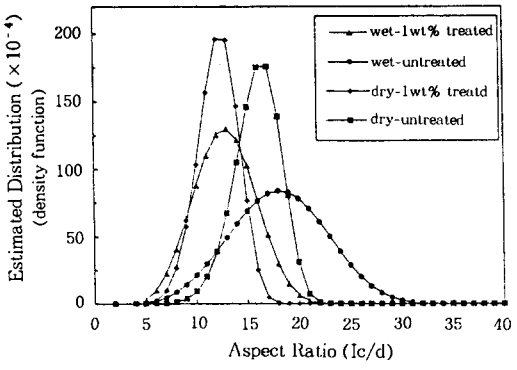

Figure 10. Comparison of the ultimate aspect ratio of fiber fragment in DFC specimens for the treated and the treated fibers under the dry and wet conditions.

Table 4. Weibull Distribution Parameters for the Aspect Ratio (L_c/d) at the Untreated and the Amino-silane Treated SiC Fibers under Dry and Wet Conditions

conc. (wt%)	aspect ratio (L_c/d)	shape parameter (β)	scale parameter (α)	IFSS (MPa)
dry				
untreated	154	134	6.5	15.4
0.5	136	110	10.9	26.7
1	105	93	5.1	39.5
2	144	120	7.5	23.1
5	154	127	9.1	20.4
wet				
untreated	145	161	3.5	14.0
0.5	112	122	5.1	26.0
1	93	103	3.5	37.8
2	121	131	5.3	21.9
5	181	198	4.6	13.0

* Gauge length : 2 mm.
* Used estimator : $F(X_i)=i/N+1$.

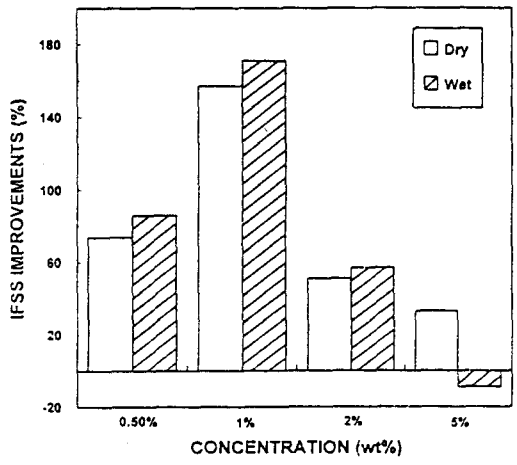

Figure 11. Improvement % in IFSS of SiC fibers treated with the amino-silane coupling agent under dry and wet conditions, compared with the untreated case.

ered to explain the improved IFSS. First, interphase I can be between the fiber surface andthe silane coupling agent. There can be the siloxane bonding (Si-O-Si) between the hydroxy group in SiC fiber surface and the silanol group in the silane coupling agent. Second, interphase II may be considered between amino-silane coupling agent and PC matrix. There can be a secondary H-bonding, covalent bonding and physical adhesion by interdiffusion between the PC matrix and amino-silane. Those interacting forces can contribute to improve the IFSS. Fig. 12 illustrated schematic figure showing possible ways of chemical bonding contributing to the interfacial adhesion between SiC fiber and PC matrix using amino-silane coupling agent. Fig. 12(a) showed hydrogen bonding between silane and SiC fibers, then following polysiloxane bonding in Fig. 12(b). The schematic interdiffusion between silane and PC matrix can be shown in Fig. 12(c).

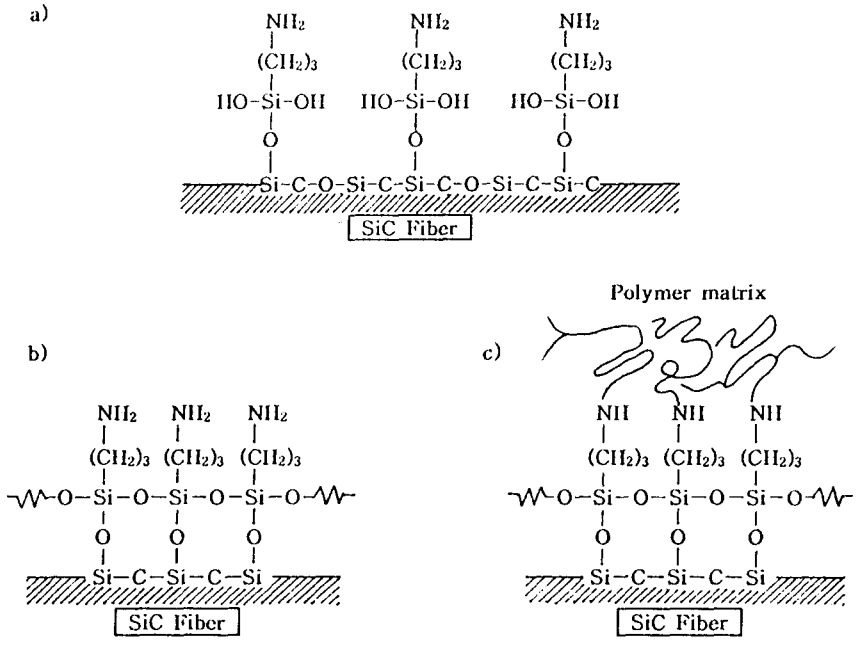

Figure 12. Schematic illustration showing possible ways of chemical bonding contributing to the interfacial adhesion between SiC fiber and polycarbonate matrix using silane coupling agent.

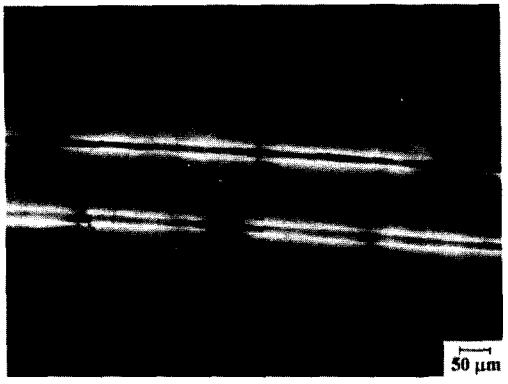

Figure 13. Optical photograph of the untreated (upper) and 1 wt% amino-silane treated (down) SiC fibers/polycarbonate specimen with polarized-light.

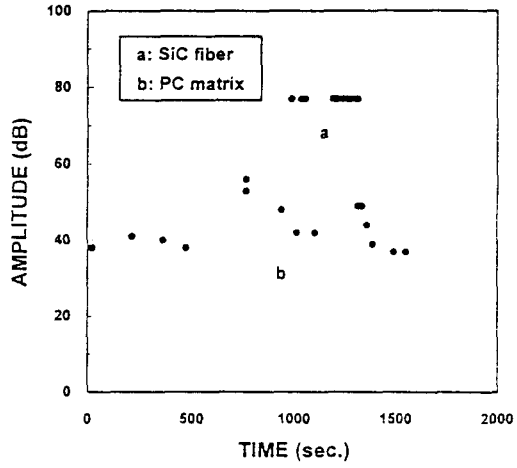

Figure 14. AE peak amplitude for SiC fiber embedded SFC specimen as a function of measuring time.

Fig. 13 showed the birefringence pattern of DFC specimen for the untreated and 1 wt% silane treated SiC fibers embedded in a same PC matrix together. Fiber fragment lengths treated with 1 wt% amino-silane are shown to be relatively shorter than the untreated case, which means the higher IFSS between fiber and matrix due to the Kelly and Tyson equation. This can show the direct-distinct comparison between the untreated and the treated at the same conditions, such as matrix, tensile testing rate etc. It also can save experimental time.

AE Analysis Using DFC Specimens and Correlation with the IFSS. In addition to the direct observation of the fiber fragmentation via an optical microscopy, AE activity was also monitored by a piezoelectric transducer positioned at the center of the DFC specimen. It was of interest to know the sequence of fiber fracture and micro-cracking of PC matrix in the specimen for the correlation of the AE events with the different micro-failure sources.

Fig. 14 showed the AE peak amplitude for single SiC fiber as a function of measuring time. Each groups were well separated into two different ranges of the AE amplitude, which are lower range of 40-60 dB and higher range of 78 dB above. The value of peak amplitude being larger than 78 dB was indicated to 78 dB because of system dynamic range in this experiment. Matrix cracking was shown in the lower AE amplitude range, whereas fiber breakages were in higher AE amplitude range. Before fiber starts to break, the matrix cracks first due to micro-defects or voids inside the matrix.

Fig. 15 also showed two distinct groups in the distribution of AE peak amplitude and AE energy for SiC fiber/PC specimen. Generally, the true energy is directly propotional to the area under the acoustic emission waveform. The electrical AE energy can be defined as

$$\text{AE Energy} = (1/R) \int_0^\infty V^2(t)\, dt \qquad (10)$$

where R is the electrical resistance of the measuring circuit, and $V(t)$ is the output voltage of the transducer which is closely related to AE amplitude.[22] Therefore, the AE energy distribution was spread more widely than the AE peak amplitude, because the AE energy was related

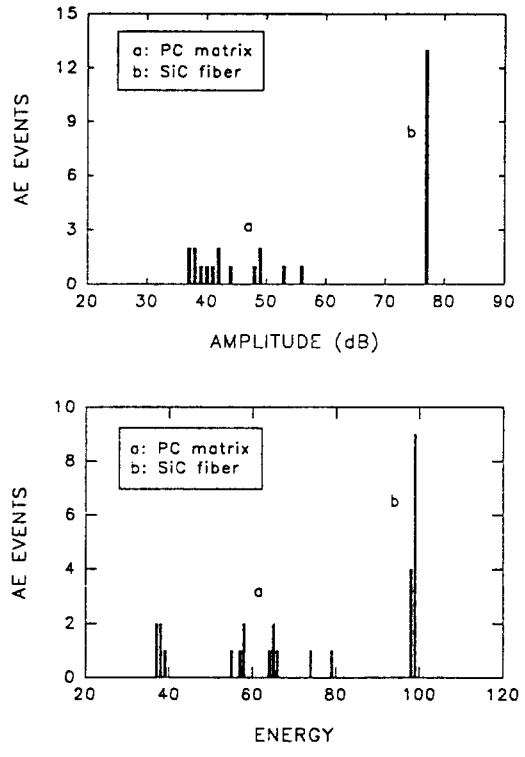

Figure 15. Distribution of events by peak amplitude and energy in SiC fiber embedded SFC specimen.

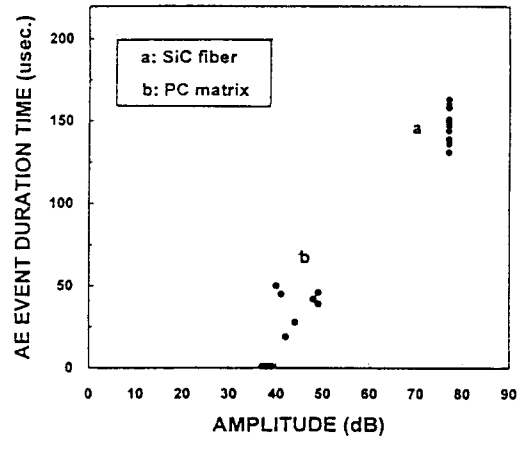

Figure 16. AE event duration time versus AE peak amplitude for SiC fiber embedded SFC specimen.

to the signal amplitude and signal duration.

As an additional analysis, the cross-plot of AE event duration time versus AE peak amplitude was made for SiC fiber embedded SFC specimen in Fig. 16. It can be shown that group (a) indicates large energy signals with large amplitude and large event duration due to fiber breakages, whereas group (b) indicates small energy signals with small amplitude and small event duration by matrix crackings. These results can be confirmed in the following waveform analysis.

Fig. 17 showed typical AE waveforms generated during a tensile test and their fast Fourier transform (FFT) results. As mentioned before, these typical waveforms can also be divided into two groups. One is large energy signal due to SiC fiber breakage, and the other is small energy signals resullting from the PC matrix cracking. In the case of SiC fiber breakage, the characteristic peaks appear in the unique frequency at about 270 kHz. On the other hand, several peaks appear in the 250-600 kHz frequency ranges including relatively high 270 kHz peak due to PC matrix cracking. From this analysis, it can be known that the AE signals with high frequency components may be generated from matrix cracking rather than fiber breakage, comparatively.

Fig. 18 showed a one-to-one correspondence between the fiber breakages and AE events based on the well separated AE events distributions. This correlation can be obtained from the fiber fracture observed microscopically and the subsequently accompanying AE events. The reason for slight larger number of AE events is because AE signal also detected from the fiber breakage within both grip lengths, whereas the number of fiber breakage was counted only within gauge length via optical microscopy. The number of the untreated fiber breakage was in the range of 15 to 19 via optical microscope. It is probably due to statistically different diame-

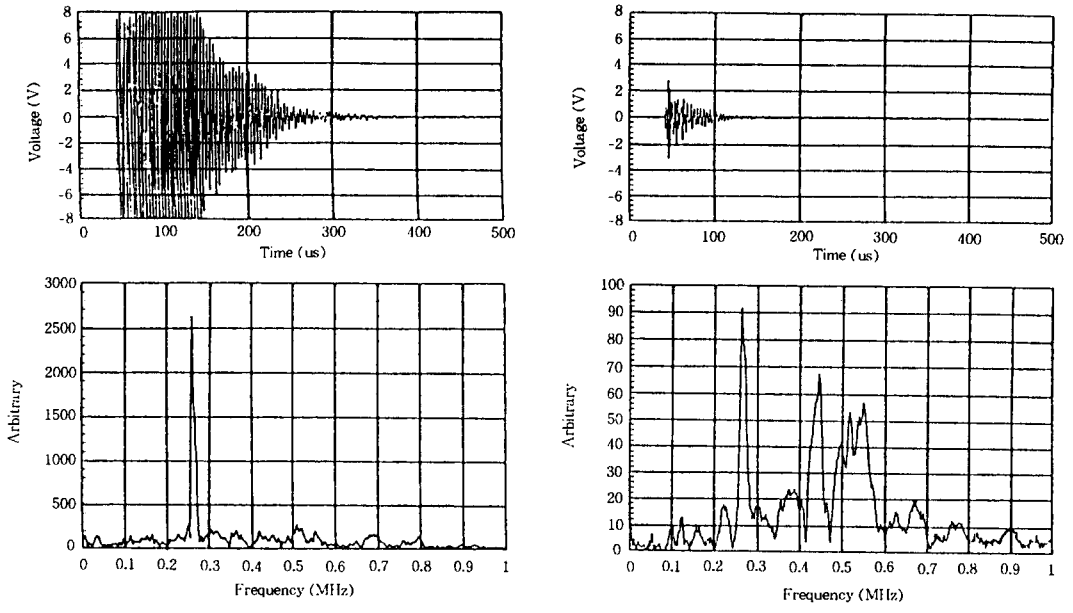

Figure 17. AE waveforms and their FFT results obtained from SiC fiber/polycarbonate composite specimen while straining.

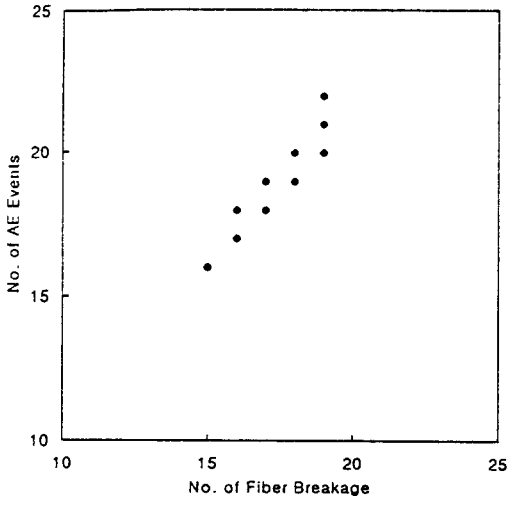

Figure 18. A one-to-one correspondence between the number of fiber breakage and the number of AE event for the DFC specimens.

ter ranges of SiC fiber and randomly existing flaws. As the diameter increases, the number of AE event and fiber breakage becomes to be decreased. This comes from directly the relationship that the critical aspect ratio, L_c/d is equal to $\sigma_f/2\tau$ assuming a constant IFSS.

From these results, if the fiber breakage group can be well separated from the matrix cracking by adjusting AE threshold, AE method can be utilized to calculate the IFSS more easily by avoiding such a tedious counting procedure through an optical microscopy. It also can be applied in especially opaque or dark-colored thermoplastic or thermosetting composites, where it is impossible to observe.

CONCLUSIONS

Effects on amino-silane coupling agent of the interfacial shear strength (IFSS) for dual SiC fibers reinforced PC composites (DFC) were investigated via fragmentation test and acoustic emission methods. Obtained results are as follows:

- Tensile strength and elongation for SiC fiber

decreased with increasing gauge lengths, due to heterogeneous distribution of flaws on the fiber surface.

- Large improvements in the IFSS by amino-silane treatment were shown under both dry and wet conditions, due to chemical bonding and/or physical bonding in two interphases.
- In the DFC specimens two distinct distribution groups were exhibited from AE analysis. The range from fiber breakage was well separated from the range of the matrix cracking. Also characteristic peak frequencies from fiber breakages and matrix cracking failures were observed by the FFT analysis. Clear difference in AE signals indicates two different types of failure mechanism.
- A one-to-one correspondence between AE events and fiber breakages has been established for SiC fiber/PC composites specimens. AE method can be applied as another method to calculate the IFSS more easily in especially opaque or dark-colored thermoplastic or thermosetting composites.

Acknowledgements: This study was supported by the Korea Science Engineering Foundation (KSEF Grant No. 951-0848-002-1).

REFERENCES

1. R. C. Harper, *SAMPE J.*, **28**(2), 9 (1992).
2. L. S. Schadler, C. Laird, and J. C. Figueroa, *J. Materials Sci.*, **27**, 4024 (1992).
3. C. C. M. Ma, C. L. Lee, M. J. Chang, and N. H. Tai, *Polymer Composites*, **13**, 448 (1992).
4. J. K. Deporter, D. G. Baird, and G. L. Wilkes, *Rev. Macromol. Chem. Phys.*, **C33**, 1 (1993).
5. J. M. Park and R. V. Subramanian, *J. Adhesion Sci. & Technol.*, **5**, 459 (1991).
6. J. M. Park, R. V. Subramanian, and A. E. Bayoumi, *J. Adhesion Sci. & Technol.*, **8**, 133 (1994).
7. T. Kobayashi, S. Takahashi, and N. Fuji, *J. Appl. Polymer Sci.*, **49**, 417 (1993).
8. A. R. Sanadi and M. R. Piggott, *J. Mater. Sci.*, **20**, 431 (1985).
9. J. M. Park, J. H. Lee, and D. J. Yoon, *Proceedings of the 10th International Conf. on Composite Materials (ICCM)*, VI, 573 (1995).
10. A. N. Netravali, R. B. Henstenberg, S. L. Phoenix, and P. Schwartz, *Polymer Composites*, **10**(4), 226 (1989).
11. A. N. Netravali, D. Stone, S. Ruoff, and T. T. T. Topoleski, *Composites Sci. and Technol.*, **34**, 289 (1989).
12. A. Kelly and W. R. V. Tyson, *Mech. and Phys. of Solids*, **13**, 329 (1965).
13. A. S. Wimolkiatisak and J. P. Bell, *Polymer Composites*, **10**, 162 (1989).
14. L. T. Drzal, M. J. Rich, M. F. Koenig, and P. F. Lloyd, *J. of Adhesion*, **16**, 133 (1983).
15. B. T. Ma, L. S. Schadler, C. Laird, and J. C. Figueroa, *Polymer Composites*, **11**(4), 211 (1990).
16. E. V. Pisanova, S. F. Zhandarov, and V. A. Dovgyalo, *Polymer Composites*, **15**(2), 147 (1994).
17. T. Ishikawa, *Composites Sci. and Technol.*, **51**, 134 (1994).
18. C. P. Beetz. Jr., *Fiber Sci. and Technol.*, **16**, 45 (1982).
19. H. F. Wu and A. N. Netravali, *J. Mater. Sci.*, **27**, 3318 (1992).
20. W. Sachse, A. N. Netravali, and A. R. Baker, *J. Nondestruc. Eval.*, **11**, 251 (1993).
21. K. Goda and H. Fukunaga, *J. Mater. Sci.*, **21**, 4475 (1986).
22. R. Kline, "Acoustic Emission Signal Characterization, in Acoustic Emission", ed. by J. R. Matthews p. 105, Gordon and Breach Science Publishers Inc., New York, 1983.